Progress In Electromagnetics Research, PIER 53, 249–269, 2005

EXCITATION AND DETECTION OF WAVES IN THE FDTD ANALYSIS OF N-PORT NETWORKS

J. L. Young and R. Adams

Department of Electrical and Computer Engineering
University of Idaho
Moscow, ID 83844-1023, USA

Abstract—An FDTD methodology is provided herein that allows for TEM excitation and detection of signals associated with N-port network analysis. The scheme is based upon the numerical solution of Laplace's equation in the context of the standard Yee grid. The invocation of both equivalence and orthogonality of modes principles assures that the TEM mode of interest is both exclusively excited and detected. Electric and magnetic surface currents are employed to render zero backward radiation from the source plane. Orthogonality is utilized at the terminal plane to extract the TEM mode from a multi-mode signal, provided that the spectrum of the guiding structure is discrete. The advantage of this approach is found in the placement of both the terminal and source planes — both can be placed as close to each other and to the network as necessary, thus alleviating the computational and memory burdens of the simulation. Examples pertaining to this methodology include stripline structures and the monopole strip antenna. The microstrip patch antenna is also considered to demonstrate the difficulties associated with the excitation and detection of quasi-TEM signals in the midst of radiation terms.

Acknowledgment

References

1. INTRODUCTION

An electromagnetic problem suitable to numerical analysis is the N-port network, referred to in this paper as the device under investigation (DUI). Each port of the network is defined in terms of a terminal and source plane on some transmission line or waveguide, as shown in Figure 1. (An antenna is regarded as a one-port network in this paper.) To properly characterize the DUI in terms of a linear combination of port voltages and/or currents, it is imperative that it is done in the context of a particular mode of operation [1], usually the dominant mode of the waveguide. For homogeneous, two-conductor waveguides, such as the stripline and the coaxial cable, the dominant mode is the TEM mode; for inhomogeneous structures, such as the microstrip, it is the quasi-TEM mode.

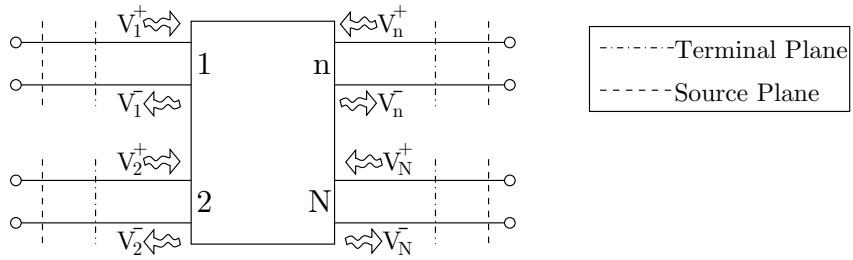

Figure 1. An N-port network.

A typical method for exciting the dominant mode at the source plane is to place soft or hard sources in the vicinity of the conductors that form the waveguide [2–4]. Depending upon their configuration, these sources will accomplish their intended purpose with some efficacy, with the additional outcome of exciting higher order modes, radiation waves and surface waves, if such modes or waves are part of the waveguide's spectrum of operation. Unfortunately, these undesirable modes and waves can adversely interact with the DUI if the waveguide propagates more than one mode or if the source plane is placed too close to the DUI. When such interactions occur, a unique characterization of the network is difficult.

With respect to the detection of TEM signals at the terminal plane, the standard practice is to integrate the electric intensity along

some line (that lies in the plane of the terminal plane) between the two conductors of the waveguide to obtain the voltage between the conductors [5]. This approach is valid if the waveguide is exclusively guiding a TEM wave at the terminal plane, in which case the voltage is independent of the integration path. However, if other modes or radiation fields are created by the network, the voltage will be path dependent and hence, not unique. Similarly, by means of Ampere's law, the conduction current is typically obtained by integrating the magnetic intensity on some closed path on the terminal plane about the conductor [5]. If longitudinal displacement currents exist, then the result of that integration will be the total current, not the desired conduction current, whose value also depends on the path of integration. Thus, when higher order modes or radiation fields exist at the terminal plane, the concept of voltage and current is ambiguous and the network parameters based on these voltages and currents are invalid. The natural, but impractical, way to assure valid computation of the port voltages and currents is to place the terminal plane "far" from the DUI in hope that all non-TEM terms are negligible.

An unambiguous characterization of the DUI requires not only a precise understanding of both the excitation field at the source plane and the response field at the terminal plane but also a recipe for where the source and terminal planes can be placed to get valid terminal plane data [6]. To avoid the excitation of unwanted modes and fields, impressed electric and magnetic surface currents on the source plane can be designed to couple exclusively to the mode of interest by means of equivalence principles. For example, if $\boldsymbol{E}_{ta}$ and $\boldsymbol{H}_{ta}$ are the transverse electric and magnetic intensities of the ath mode, as obtained from the homogeneous solution of Maxwell's equations for some waveguiding structure, then the ath mode is exclusively excited if electric and magnetic surface currents are defined as $\boldsymbol{n} \times \boldsymbol{H}_{ta}$ and $\boldsymbol{E}_{ta} \times \boldsymbol{n}$, respectively, on the source plane. Here $\boldsymbol{n}$ is the unit normal vector in the direction of propagation. Although only one impressed source is needed to excite the desired mode, both are used to assure a null field behind the source plane, per the equivalence theorem [7]. The null field attribute allows the terminal plane to be placed in front of or behind the source plane, depending on whether the scheme is to be regarded as a total or scattered field formulation. When the mode of interest is the TEM mode, the homogeneous solution is constructed using static potential theory. In the context of an FDTD algorithm, the potential solution can be found using a finite difference procedure in conjunction with the standard Yee grid, as shown herein. This excitation procedure has some commonality with presimulation and mode template methods [8, 9], but does not require single mode

waveguide operation.

With respect to the detection problem, these same transverse fields $\boldsymbol{E}_{ta}$ and $\boldsymbol{H}_{ta}$ can be used in conjunction with modal orthogonality to isolate the mode of interest from the total signal [1, 10, 11]. If the mode of interest is the TEM mode, then the results from orthogonality can be used to find unique terminal plane voltages and currents. Moreover, when current sheet excitation is used in conjunction with orthogonal mode detection, the source and terminal planes can be placed arbitrarily close to each other.

The significant obstacle to detecting the mode of interest (TEM, TM or TE) is isolating that mode from the total signal when modal orthogonality is not valid. This can occur, for example, with open transmission lines such as the parallel wire or the microstrip. Consider the former connected to a center-fed, half-wave dipole. The parallel wire does support the TEM mode, which can be exclusively excited using properly defined impressed current sheets. The excited TEM wave will travel towards the dipole, with some of the incident signal coupling to the dipole's radiation field and some of the remaining signal reflecting back towards the source plane in terms of TEM, TE and/or TM modes. If that were the entire picture, then the mode of interest could be extracted from the reflected signal by means of orthogonality. Unfortunately, the parallel wire's spectrum is comprised of a radiation field that is excited by the dipole. The presence of the radiation field renders the isolation of the mode of interest from the total signal by means of orthogonality ineffectual. (The same would hold true using simple line integral methods.) Other than moving the terminal plane infinitely far from the dipole, where the radiation field is negligible in comparison to the propagating mode (assuming of course, a lossless line), it appears for this case that no unambiguous method exists for uniquely characterizing the signal at the terminal plane. The conundrum of this example, of course, is that the transmission line and the dipole cannot be considered as two distinct pieces of hardware. A similar discussion can be applied to the microstrip-fed patch antenna, with one additional difficulty: the quasi-TEM mode is not exclusively excited using the electrostatic potential. On the other hand, the coaxially-fed monopole is quite easy to characterize using modal orthogonality, given that the coax is a closed waveguide that supports only orthogonal modes.

Examples such as the coaxial monopole and the microstrip-fed patch are provided in this paper to demonstrate the salient features of the theory. The theory is couched in terms of the numerical FDTD algorithm, but is in nowise restricted to this one algorithm, numerical or otherwise.

2. TEM EXCITATION

Consider a lossless, two-conductor waveguide that is surrounded by a homogeneous material. It is well known that this waveguide supports a TEM wave that can be represented in terms of a transverse static field and a longitudinal propagation factor $f(t-z/v_p)$, for propagation in the positive z-direction at a phase speed of v_p [1]. For the electric intensity $\boldsymbol{E}$, that representation is

$$\boldsymbol{E} = \boldsymbol{E}_{ts} f(t - z/v_p), \tag{1}$$

where $\boldsymbol{E}_{ts}$ is the transverse static electric intensity, which, for Cartesian coordinates, is given by

$$\boldsymbol{E}_{ts} = E_{xs}\boldsymbol{a}_x + E_{ys}\boldsymbol{a}_y = -\nabla_t \phi = -\left(\frac{\partial}{\partial x}\boldsymbol{a}_x + \frac{\partial}{\partial y}\boldsymbol{a}_y\right)\phi. \tag{2}$$

Here $\phi = \phi(x, y)$ is the electrostatic potential in the transverse plane, which is a solution to Laplace's equation,

$$\nabla_t \cdot (\epsilon \nabla_t \phi) = 0. \tag{3}$$

In the preceding equations, ∇_t is the transverse del operator and ϵ is the permittivity of the material. For homogeneous materials, the previous equation reduces to $\nabla^2\phi = 0$ and $\boldsymbol{E}$ of Eqn. (1) is an exact solution to Maxwell's equations. For inhomogeneous materials, $\boldsymbol{E}$ is not a valid solution to Maxwell's equations; it may be, however, an approximate solution for the quasi-static TEM mode, under certain circumstances [12]. The potential is also subject to the boundary condition

$$\phi = V_n \tag{4}$$

on conductor n, where $n = 1, 2, \ldots, N$ of an N conductor system. For example, for a balanced shielded-pair, $N = 3$ with the shield set to ground potential and the two inner conductors set to $\pm V_s/2$ Volts, where V_s is the voltage between the two inner conductors. As for the magnetic intensity $\boldsymbol{H}$, we write

$$\boldsymbol{H} = \boldsymbol{H}_{ts} f(t - z/v_p), \tag{5}$$

where $\boldsymbol{H}_{ts}$ is the transverse static magnetic intensity:

$$\boldsymbol{H}_{ts} = H_{xs}\boldsymbol{a}_x + H_{ys}\boldsymbol{a}_y = -\frac{1}{\eta}\boldsymbol{a}_z \times \nabla_t \phi, \tag{6}$$

with η being the characteristic impedance of the material that supports the waveguide's conductors.

One way to excite these TEM fields is to establish a set of impressed current sheets $\boldsymbol{J}_s$ and $\boldsymbol{M}_s$ on the $z = z_0$ plane in accordance with equivalence principles:

$$\boldsymbol{J}_s = \boldsymbol{a}_z \times \boldsymbol{H}\Big|_{z=z_0} = (H_{xs}\boldsymbol{a}_y - H_{ys}\boldsymbol{a}_x) f(t - z_0/v_p) \tag{7}$$

and

$$\boldsymbol{M}_s = \boldsymbol{E} \times \boldsymbol{a}_z\Big|_{z=z_0} = (E_{ys}\boldsymbol{a}_x - E_{xs}\boldsymbol{a}_y) f(t - z_0/v_p). \tag{8}$$

Per the equivalence theorem, these currents are assured to create the $\boldsymbol{E}$ and $\boldsymbol{H}$ fields of Eqns. (1) and (5) in the region $z > z_0$ and the null field in the region $z < z_0$ [7]. It should be noted that both $\boldsymbol{J}$ and $\boldsymbol{M}$ are not needed to create a forward going wave. The presence of both only ensures a zero negative going wave; the omission of either $\boldsymbol{J}$ and $\boldsymbol{M}$ will result in both a forward and negative going wave emanating from the source plane.

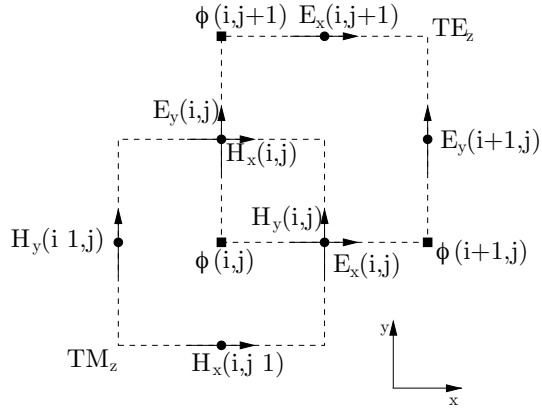

Figure 2. The two-dimensional (2D) TE-to-z and TM-to-z Yee cells.

The crux of creating the aforementioned impressed currents relies on finding the solution to Eqns. (3) and (4) numerically, or otherwise. To solve Laplace's equation numerically, a finite-difference approach is invoked in conjunction with the grid of Figure 2. The potential is located in the center of the TM_z two-dimensional (2D) Yee cell with the magnetic intensity components placed about it in accordance with the standard FDTD procedure. The potential is also located at the vertices of the TE_z 2D Yee cell with the electric intensity components placed about it in accordance with the standard FDTD procedure. Even though these two 2D cells are displaced from one another in z by a half cell in the standard 3D cell, this is of no consequence in the calculation

of the static fields since ϕ is not a function of z - the cell displacement is accounted for in the propagation factor $f(t-z/v_p)$. Using the index scheme of Figure 2 and the central difference representation of the Laplacian, we approximate Eqn. (3) with

$$\alpha_1\phi_{i-1,j} + \alpha_2\phi_{i,j-1} + \alpha_3\phi_{i,j} + \alpha_4\phi_{i,j+1} + \alpha_5\phi_{i+1,j} = 0, \tag{9}$$

where $\phi_{i,j}$ denotes the value of ϕ at node i,j. Also, $\alpha_1 = \epsilon_{i-1/2,j}/\delta_x^2$, $\alpha_2 = \epsilon_{i,j-1/2}/\delta_y^2$, $\alpha_4 = \epsilon_{i,j+1/2}/\delta_y^2$, $\alpha_5 = \epsilon_{i+1/2,j}/\delta_x^2$ and

$$\alpha_3 = -\frac{\epsilon_{i+1/2,j} + \epsilon_{i-1/2,j}}{\delta_x^2} - \frac{\epsilon_{i,j+1/2} + \epsilon_{i,j-1/2}}{\delta_y^2}; \tag{10}$$

here δ_x and δ_y are cell lengths. In the above equations, $\epsilon_{i-1/2,j}$, for example, denotes the value of the permittivity half way between the potential nodes i,j and $i-1,j$. For homogeneous media, the permittivity is constant and common among all the Laplacian coefficients; for this case, the permittivity terms can be omitted. Eqn. (9) is applied to every interior node in the domain. For boundary nodes, we replace Eqn. (9) with $\phi_{i,j} = V_{i,j}$, where $V_{i,j}$ is the impressed voltage at node i,j. The system of equations produced by Eqn. (9) and the boundary equations is solved once at the beginning of the simulation using standard iterative techniques of sparse matrices. Given that the system characterizes a two-dimensional domain, the overhead in computing $\phi_{i,j}$ is trivial.

Once ϕ is known at every point in the transverse plane, the static fields are calculated using central differences. From Eqns. (2) and (6) and from Figure 2,

$$E_{xs}(i,j) = \eta H_{ys}(i,j) \approx -\frac{\phi_{i+1,j} - \phi_{i,j}}{\delta_x} \tag{11}$$

and

$$E_{ys}(i,j) = -\eta H_{xs}(i,j) \approx -\frac{\phi_{i,j+1} - \phi_{i,j}}{\delta_y}. \tag{12}$$

Finally, the components of the impressed currents are conjoined with the components of the previous static field on the Yee grid in the following manner: $J_{xs}(i,j) = -H_{ys}(i,j)$, $J_{ys}(i,j) = H_{xs}(i,j)$, $M_{xs}(i,j) = E_{ys}(i,j)$ and $M_{ys}(i,j) = -E_{xs}(i,j)$.

With the transverse impressed currents so determined, the final step is to incorporate these currents in the leap-frog integration scheme similar to that of [13]. This is accomplished by delaying one current density by a half time-step relative to the other. With δ_t being the time step, the integrated form of Maxwell's equations becomes

$$\epsilon \boldsymbol{E}^{n+1/2} = \epsilon \boldsymbol{E}^{n-1/2} + \delta_t \nabla \times \boldsymbol{H}^n - \delta_t \boldsymbol{J}_s^n \tag{13}$$

and

$$\mu \boldsymbol{H}^{n+1} = \mu \boldsymbol{H}^{n} - \delta_t \nabla \times \boldsymbol{E}^{n+1/2} - \delta_t \boldsymbol{M}_s^{n+1/2}, \tag{14}$$

where it is understood that the source plane for $\boldsymbol{J}_s$ is one half cell away from the source plane for $\boldsymbol{M}_s$. Given that the static transverse fields are computed once at the beginning of the simulation and stored for future use, the computational burden of incorporating the impressed currents into Maxwell's equations is negligible.

The final step in the implementation of the excitation scheme is to compute the value of v_p from the potential function. (Recall that v_p is needed in the propagation factors in Eqns. (7) and (8)). Moreover, in anticipation of some information needed in the detection scheme, the potential can also be used to compute the waveguide's characteristic impedance, inductance per unit length, capacitance per unit length and effective permittivity as follows. Consider a typical two conductor transmission line with one conductor fixed at a known potential V_s and the other held at zero potential. By definition,

$$V_s = -\int_{l_1} \boldsymbol{E}_{ts} \cdot d\boldsymbol{l}, \tag{15}$$

where l_1 is any path between the two conductors. With the static magnetic intensity known from the potential function, it can be integrated about the conductor to find the TEM conduction current I_s, per Ampere's law — to wit,

$$I_s = \oint_{l_2} \boldsymbol{H}_{ts} \cdot d\boldsymbol{l}, \tag{16}$$

where l_2 is any path about one of the conductors in the sense of the right hand rule. The conductor's potential V_s divided by its current I_s is the characteristic impedance Z_0 of the transmission line. The potential function can be used to construct the normal component of the electric intensity next to the conductor; this component is proportional to the charge density, per Gauss's law. The charge density is integrated about the conductor to find the total charge on the conductor Q_s, which is subsequently used to find the capacitance C via Q_s/V_s. The inductance L, phase speed v_p and effective permittivity ϵ_e of the material are computed using the following: $L = CZ_0^2$, $v_p = 1/\sqrt{LC}$ and $\epsilon_e = (c/v_p)^2$, where c is the speed of light [14]. All of these quantities (i.e., I_s, Z_0, etc.) are computed once at the beginning of the simulation; two of these quantities (i.e., V_s and I_s) are used in the detection scheme, as described next.

3. TEM DETECTION

To detect the TEM mode in the midst of other modes, the principle of modal orthogonality is invoked. This is accomplished by recognizing that the transverse fields of a closed transmission line (i.e., coaxial cable, stripline, shielded pair, etc.) with an arbitrary cross-sectional shape S, a homogeneous dielectric, and no conduction losses can be represented in terms of a weighted sum of orthogonal wave functions at the terminal plane [1]:

$$\boldsymbol{E}_t = \sum_a B_a \boldsymbol{E}_{ta} \tag{17}$$

and

$$\boldsymbol{H}_t = \sum_a C_a \boldsymbol{H}_{ta}, \tag{18}$$

where $\boldsymbol{E}_{ta}$ and $\boldsymbol{H}_{ta}$ are transverse mode functions of the ath mode and $\boldsymbol{E}_t$ and $\boldsymbol{H}_t$ are the total transverse fields of the simulation at the terminal plane. The excitation coefficients B_a and C_a are frequency dependent, except for the TEM mode. The TEM mode will be identified as $a = s$ and the transverse mode functions for the same are given by Eqns. (2) and (6). By making use of the inner product

$$< \boldsymbol{E}_{ta}, \boldsymbol{E}_{tb} > \equiv \int_S \boldsymbol{E}_{ta} \cdot \boldsymbol{E}_{tb} dS, \tag{19}$$

and the orthogonality relationship

$$< \boldsymbol{E}_{ta}, \boldsymbol{E}_{tb} > \equiv 0 \quad \text{for } a \neq b, \tag{20}$$

we note that

$$B_a = \frac{< \boldsymbol{E}_t, \boldsymbol{E}_{ta} >}{\|\boldsymbol{E}_{ta}\|^2}, \tag{21}$$

where $\|\boldsymbol{E}_{ta}\|^2 \equiv < \boldsymbol{E}_{ta}, \boldsymbol{E}_{ta} >$ [15]. Similarly,

$$C_a = \frac{< \boldsymbol{H}_t, \boldsymbol{H}_{ta} >}{\|\boldsymbol{H}_{ta}\|^2}. \tag{22}$$

The method of computing the aforementioned inner products is accomplished by a double summation of weighted stair-step and piecewise linear functions; the weights are the values of the nodal fields on the grid [10]. For example,

$$< E_x, E_{xs} > \approx \frac{\delta_x \delta_y}{2} \sum_{i=I_1}^{I_2} \sum_{j=J_1}^{J_2} E_x(i,j) E_{xs}(i,j) + E_x(i,j+1) E_{xs}(i,j+1); \tag{23}$$

here I_1, I_2, J_1 and J_2 span the cross-sectional domain of the waveguide. The norm of the electrostatic fields is computed once at the beginning of the simulation. A similar method using power orthogonality is described in [11, 16].

With the TEM modal coefficients known, the line voltages V and currents I are uniquely determined by their corresponding line integrals of electrostatics. For the voltage,

$$V = -\int_{l1} B_s \boldsymbol{E}_{ts} \cdot d\boldsymbol{l} = B_s V_s, \tag{24}$$

where V_s is the impressed electrostatic line voltage. For the current,

$$I = \oint_{l2} C_s \boldsymbol{H}_{ts} \cdot d\boldsymbol{l} = C_s I_s, \tag{25}$$

where I_s is the electrostatic line current previously computed by Eqn. (16). Hence, the crux of the detection problem rests on the numerical calculation of Eqns. (21) and (22) at the conclusion of each time step in the simulation (or whenever such information is needed). The computational resources needed, however, to compute these coefficients is negligible.

4. SOURCE AND TERMINAL PLANES

The previous excitation scheme assures that the mode under investigation is being exclusively excited with no backward wave radiation. The detection scheme assures that the mode under investigation is extracted from all other modes that comprise the signal. Thus, the location of the terminal and source planes can be placed as near to each other and as near to the DUI as needed. As such, the source plane need not be placed on the computational boundary, as suggested in [6]. If the terminal plane is placed behind the source plane, then the data recorded at the terminal plane will only be associated with reflected waves from the DUI. In this context, we may regard the source/terminal plane configuration in terms of a scattered field configuration. If the terminal plane is placed in front of the source plane, as shown in Figure 1, then the data recorded at the terminal plane will be the total signal and the configuration is total field. The incident and reflected partial voltages, V^+ and V^-, respectively, can be extracted from the total voltage V and current I via the following relationships: $V^+ = (V + IZ_0)/2$ and $V^- = (V - IZ_0)/2$. These equations assume that V or I has been temporally averaged in order to remove the $\delta_t/2$ delay between the two. The partial voltages are then used to find the scattering network parameters,

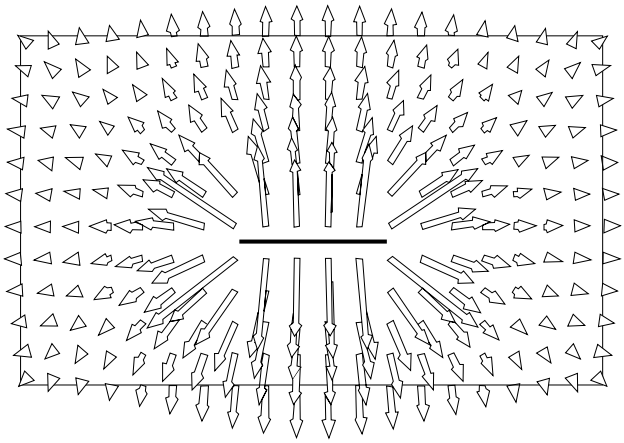

Figure 3. Field lines of transverse $\boldsymbol{E}$ on the xy-plane for surface current excitation.

provided that the transmission lines are match-terminated (or that the antenna receives no incoming radiation from the computational domain's boundary). This condition is easily satisfied by using a high quality, perfectly matched layer domain truncation scheme or absorbing boundary condition.

5. NUMERICAL RESULTS

A demonstration of the excitation scheme can be provided by considering a simple stripline geometry that is excited by a line source and by current sheets of Eqns. (7) and (8). A gaussian waveform is assumed for the pulsing function and the center strip is assumed to be z-directed and on the xz-plane. The field lines of transverse $\boldsymbol{E}$ and $\boldsymbol{H}$ for current sheet excitation, as plotted in Figures 3 and 4, respectively, have the expected fringing and circulation properties. Moreover, the strengths of E_z and H_z are a factor of 10^{-6} to that of their transverse counterparts in both early and late time data, thus substantiating the true TEM nature of the excited pulse. Although not shown, a spatial plot of $\boldsymbol{E}$ and $\boldsymbol{H}$ under the strip and as a function of strip distance reveals a pure gaussian pulse (in both early and late time) being generated at the source plane with no backward radiation. For line source excitation and as seen in Figure 5, there exists the expected coupling of the line source to the higher-order stripline modes and to the natural modes of the parallel plates that form the ground planes of the stripline. The result of this coupling is a distorted gaussian pulse

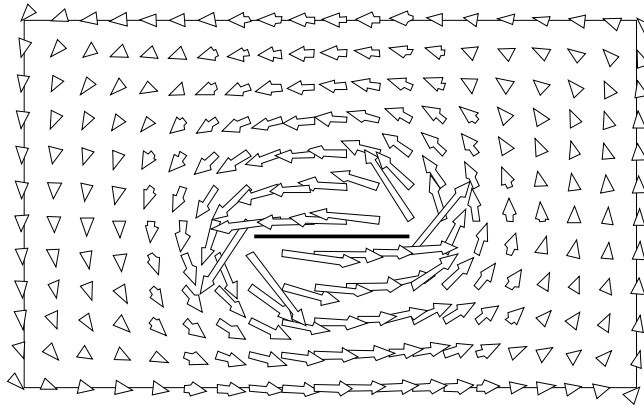

Figure 4. Field lines of transverse $\boldsymbol{H}$ on the xy-plane for surface current excitation.

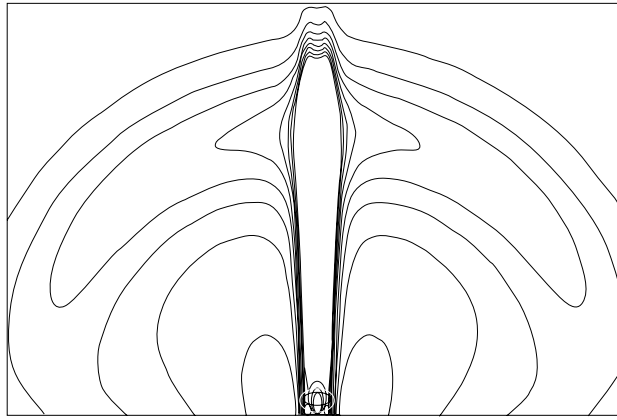

Figure 5. Contour lines of E_y on the xz-plane for line current excitation.

and bi-directional propagation.

To demonstrate the validity of the detection scheme, we examine four scenarios — two of which are associated with simple stripline geometries, one with a coaxially-fed monopole and one with a microstrip-fed rectangular patch antenna. In all cases, the DUIs are pulsed using a gaussian waveform and surface current excitation; the recorded voltage and current data are transformed into their frequency-domain counterparts using standard FFT techniques. Both

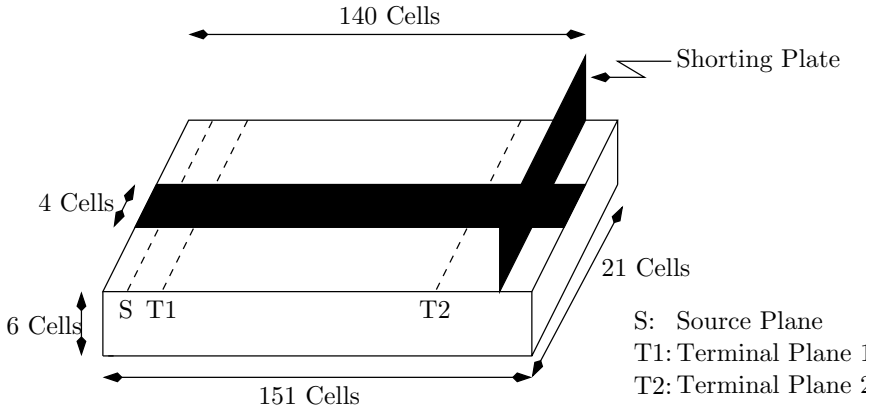

Figure 6. A transversely shorted stripline (not drawn to scale); top grounding plate not shown.

line integral detection (LID) and orthogonal integral detection (OID) are considered for the purpose of comparative analysis. Note: line integral detection refers to the traditional method of detection as discussed in the Introduction or in [5]; orthogonal integral detection refers to Eqns. (24) and (25).

Consider first Figure 6, which shows a transversely shorted stripline; the permittivity of the stripline is that of free space. Note that the short circuit is purposefully not balanced in order to excite high-order evanescent modes in the vicinity of the shorting plane by disrupting transverse $\boldsymbol{E}$. The FDTD simulation parameters are $\delta_x = 0.01\,\text{cm}$, $\delta_y = 0.01\,\text{cm}$, $\delta_z = 0.01\,\text{cm}$, and $\delta_t = 0.1\,\text{ps}$; the domain spans 21 cells in x, 151 cells in y and 13 cells in z. The frequency-domain reflection coefficient data associated with this figure are shown in Figure 7. The four reflection coefficient plots correspond to the following cases: a) terminal plane at 1 cell from the short using LID, b) terminal plane at 1 cell from the short using OID, c) terminal plane at 132 cells from the short using LID and d) terminal plane at 132 cells from the short using OID. In each of these cases, the source plane is 5 cells from the computational domain. As expected, the data shows perfect reflection for low frequencies; for high frequencies the reflection coefficient deviates from 0 dB due to the nonperfect shorting plane. More importantly, the OID method yields reflection data that are not a function of terminal plane location; the LID method yields data that are a function of terminal plane location. Both observations are consistent with expectations. The former filters out the TEM mode and since this mode does not decay, the reflection data is the same

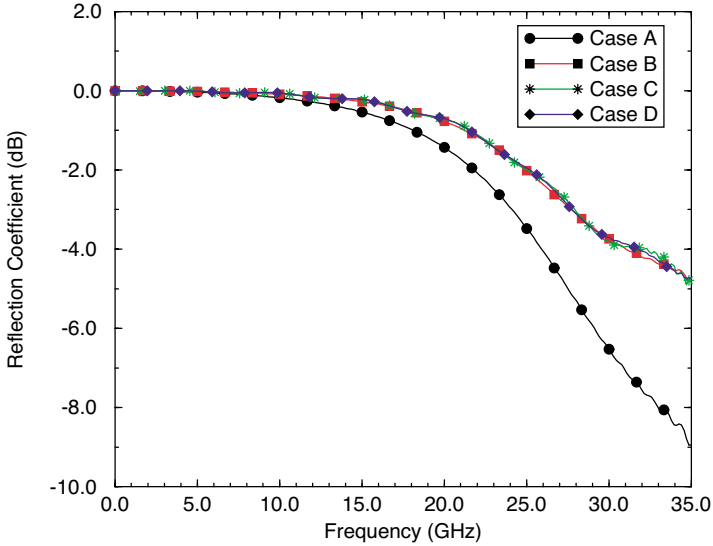

Figure 7. Reflection coefficient data for the transversely shorted strip associated with four cases: a) terminal plane at 1 cell from the short using LID, b) terminal plane at 1 cell from the short using OID, c) terminal plane at 132 cells from the short using LID and d) terminal plane at 132 cells from the short using OID.

regardless of the terminal plane location; the latter can only yield correct data when the TEM mode is exclusively propagating, which will be the case when the terminal plane is far from the short.

Using a larger computational domain, we repeated the previous experiment by considering an unbalanced short placed in the longitudinal plane in order to disrupt circulating $\boldsymbol{H}$. The reflection coefficient data associated with this case are shown in Figure 8. Similar conclusions to those made about the data for the transverse short configuration can be made for the longitudinal short. That is, the OID method yields reflection coefficient data that are independent of terminal plane placement; the LID method is terminal plane placement dependent.

The same set of numerical experiments can be made with respect to the strip monopole, as shown in Figure 9. The simulation parameters are $\delta_x = 1\,\text{cm}$, $\delta_y = 1\,\text{cm}$, $\delta_z = 1\,\text{cm}$, and $\delta_t = 9.63\,\text{ps}$; the domain spans 51 cells in x, 121 cells in y and 51 cells in z. The relative permittivity of the coaxial cable is unity. Admittance data for this structure are shown in Figure 10 for both OID and LID when

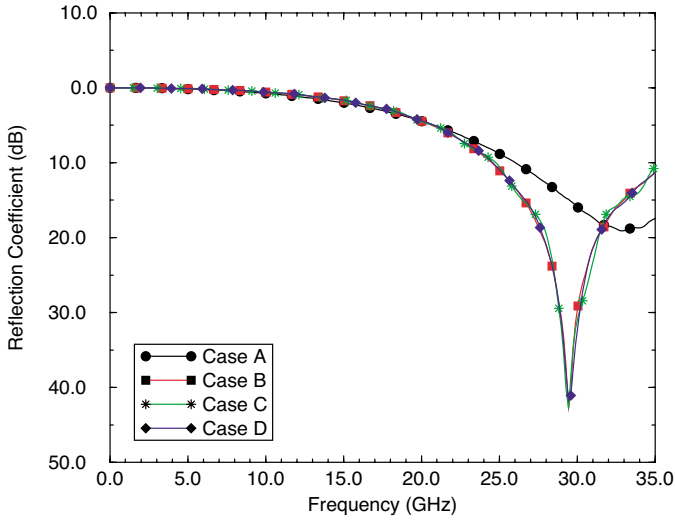

Figure 8. Reflection coefficient data for the longitudinally shorted strip associated with four cases: a) terminal plane at 1 cell from the short using LID, b) terminal plane at 1 cell from the short using OID, c) terminal plane at 232 cells from the short using LID and d) terminal plane at 232 cells from the short using OID.

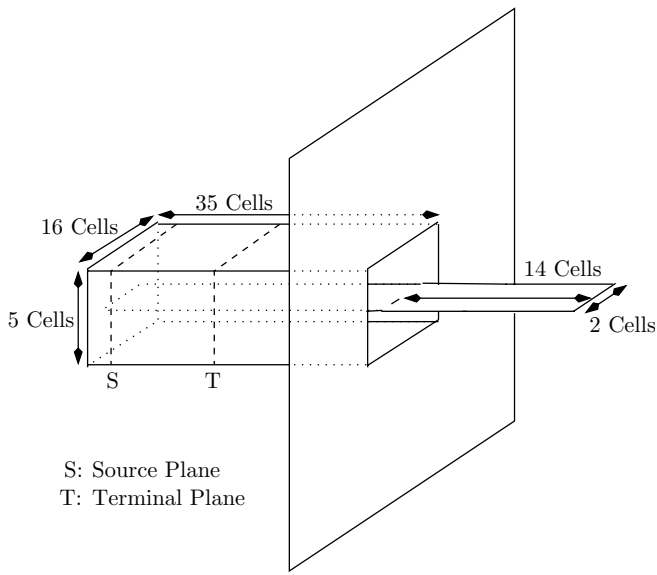

Figure 9. A strip monopole (not drawn to scale).

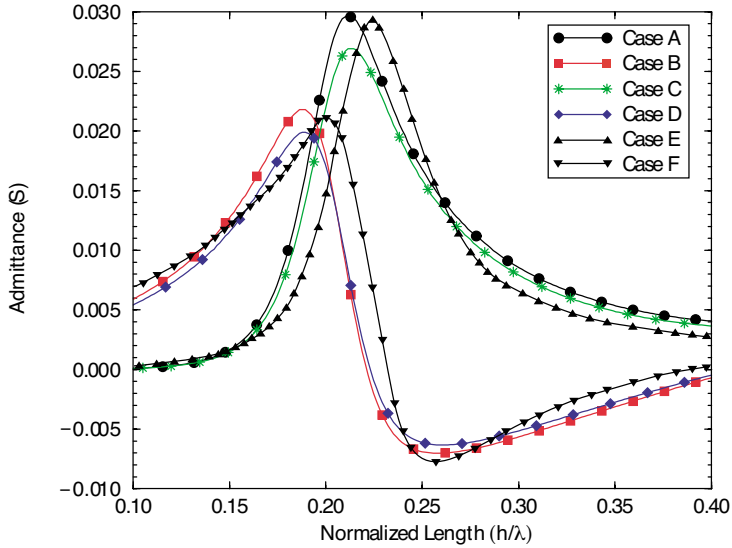

Figure 10. Admittance data for the strip monopole when the terminal plane is in the plane of the coaxial aperture. With $Y = G + jB$, the six cases are a) G data using OID, b) B data using OID c) G data using LID, d) B data using LID, e) G data from [18] and f) B data from [18].

the terminal plane coincides with the ground plane. The source plane is 5 cells from the computational boundary. Experimental data for a circular monopole (whose center wire radius is equal to the effective radius of the strip per Elliot [17] and whose characteristic impedance is the same as the strip monopole) are also plotted in Figure 10 to establish a point of reference [18]. Even with the terminal plane in the plane of the coaxial aperture where higher order modes are most strongly excited, it is clear from the plot that the OID data coincide more closely with the experimental data than the LID data. The slight shift in the resonant frequency is attributed to the differences between the circular (experimental configuration) and rectangular (FDTD configuration) cross-sectional geometries.

The final example considered in this paper is the microstrip-fed patch antenna, per the specifications of Sheen et al. [2]; see Figure 11. The simulation parameters are: $\delta_x = 0.04\,\text{cm}$, $\delta_y = 0.04\,\text{cm}$, $\delta_z = 0.0265\,\text{cm}$, and $\delta_t = 0.32\,\text{ps}$; the domain spans 61 cells in x, 101 cells in y and 17 cells in z. Reflection coefficient data associated with the following cases are plotted in Figure 12: a) terminal plane at 1

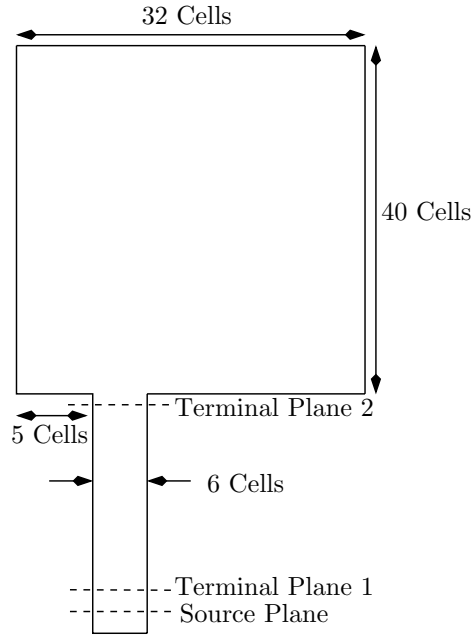

Figure 11. A microstrip-fed patch antenna (not drawn to scale).

cell from the patch using LID, b) terminal plane at 1 cell from the patch using OID, c) terminal plane at 42 cells from the patch using LID, d) terminal plane at 42 cells from the patch using OID, e) FDTD data from [2] and f) experimental data from [2]. The source plane is placed 5 cells from the computational domain. For this situation all computational methods yield slightly different results, particularly at high frequencies. And, since the microstrip does not support a pure TEM mode, all numerical results are equally right or wrong. The point in this case is that the LID method requires that the field data be TEM in order for the calculated voltages and currents to be unique; the OID method requires orthogonality among the modes, which is not the case, due to radiation and surface waves that are excited by means of reflection from the patch. The experimental data is the correct data only because the terminal plane is within the coaxial test connector, where the TEM mode exists. For the simulation results to agree with the experimental results, the simulation must include the coax-to-microstrip connector. If it does, then the OID method can be used with confidence to yield accurate data, per the many aforementioned numerical experiments.

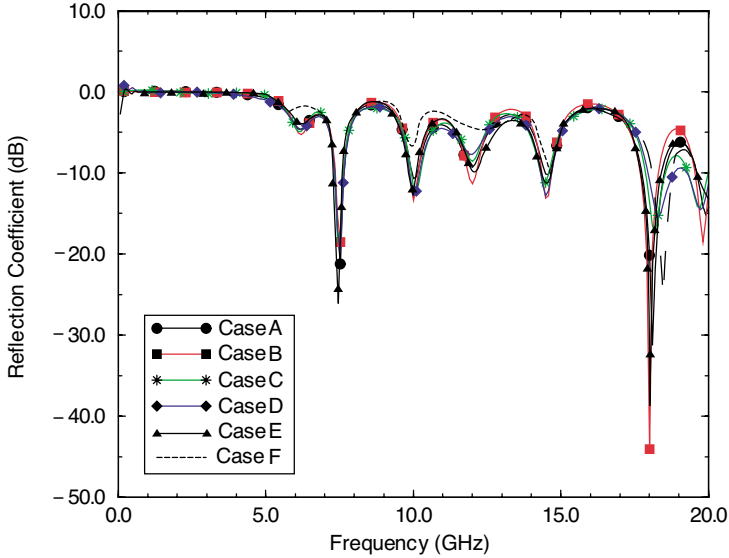

Figure 12. Reflection coefficient data for the microstrip-fed patch antenna associated with following cases: a) terminal plane at 1 cell from the patch using LID, b) terminal plane at 1 cell from the patch using OID, c) terminal plane at 42 cells from the patch using LID and d) terminal plane at 42 cells from the patch using OID, e) FDTD data from [2] and f) experimental data from [2].

6. CONCLUDING REMARKS

In this paper we have endeavored to put the excitation and detection problems of signals from N-port networks on firm footing in the context of the FDTD algorithm. Single mode excitation is assured when electric and magnetic surface currents are constructed using equivalence principles and homogeneous solutions of Maxwell's equations. Unique voltages and currents are recorded at some terminal plane using modal orthogonality, provided that the waveguide's spectrum is discrete. This excitation and detection scheme removes all ambiguity with respect to the placement of the source and terminal planes. To lessen the size of the computational domain and to minimize numerical errors such as dispersion errors, the natural choice is to place these planes as close to the DUI as possible.

The costs of employing this method are twofold. First, the computation of the orthogonal integrals relative to computation of the line integrals is more burdensome. There is also additional

computational time in the evaluation of the sheet currents relative to the evaluation of the line currents. However, for large domains, these computational burdens are insignificant relative to the computation of general FDTD equations. Second, there is additional complexity incorporated into the otherwise simple FDTD code. This complexity is found in the electrostatic pre-solver. Nonetheless, if such complexity is needed to devise a methodology that unambiguously characterizes the DUI, then we believe the extra effort is justified.

In this paper we have focussed on the TEM mode of a two-conductor waveguide. There appears, however, to be no compelling reason why the method could not be extended to include single conductor, closed waveguides that only support TE or TM modes. For these situations the modal coefficients would be frequency-dependent, which adds a convolution [19] operation to the time-domain algorithm.

ACKNOWLEDGMENT

The authors appreciate the comments of Prof. Stephen Gedney pertaining to the excitation scheme outlined in this paper and the comments of Prof. John Schneider pertaining to the paper as a whole. This work was supported by the Office of Naval Research under award number N00014-03-1-0819.

REFERENCES

1. Collin, R. G., *Field Theory of Guided Waves*, 2nd edition, IEEE Press, New York, NY, 1991.
2. Sheen, D. M., S. M. Ali, M. D. Abouzahra, and J. A. Kong, "Application of the three-dimensional finite-difference time-domain method to the analysis of planar microwave circuits," *IEEE Trans. Microwave Theory Tech.*, Vol. 38, No. 7, 849–856, 1990.
3. Luebbers, R. J. and H. S. Langdon, "A simple feed model that reduces time steps needed for FDTD antenna and microstrip calculations," *IEEE Trans. Ant. Propagat.*, Vol. 44, No. 7, 1000–1005, 1996.
4. Buechler, D. N., D. H. Roper, C. H. Durney, and D. A. Christensen, "Modeling sources in the FDTD formulation and their use in quantifying source and boundary condition errors," *IEEE Trans. Microwave Theory Tech.*, Vol. 43, No. 4, 810–814, 1995.
5. Piket-May, M., A. Taflove, and J. Baron, "FD-TD modeling of digital signal propagation in 3-D circuits with passive and active

loads," *IEEE Trans. Microwave Theory Tech.*, Vol. 42, No. 8, 1514–1523, 1994.

6. Swanson, D. G. and W. J. R. Hoefer, *Microwave Circuit Modeling Using Electromagnetic Field Simulation*, Artech House, Norwood, MA, 2003.
7. Harrington, R. F., *Time-Harmonic Fields*, McGraw-Hill, New York, NY, 1961.
8. Railton, C. J. and J. P. McGeehan, "The use of mode templates to improve the accuracy of the finite difference time domain method," *21st European Microwave Conf.*, 1278–1283, Stuttgart, Germany, 1991.
9. Celuch-Marcysiak, M., A. Kozak, and W. K. Gwarek, "A new efficient excitation scheme for the FDTD method based on the field and impedance template," *IEEE Antennas and Propagat. Soc. Int. Symp.*, Vol. 2, 1296–1299, Baltimore, MD, July 1996.
10. Craddock, I. J., D. L. Paul, C. J. Railton, P. N. Fletcher, and M. Dean, "Applications of single mode extraction from finite difference time domain data," *IEE Proc. - Microwave and Ant. Propagat.*, Vol. 146, No. 2, 160–162, 1999.
11. Gwarek, W. K. and M. Celuch-Marcysiak, "Wide-band S-parameter extraction from FDTD simulations for propagating and evanescent modes in inhomogeneous guides," *IEEE Trans. Microwave Theory Tech.*, Vol. 51, No. 8, 1920–1927, 2003.
12. Alexópoulos, N. G., "Integrated-circuit structures on anisotropic substrates," *IEEE Trans. Microwave Theory Tech.*, Vol. 33, No. 10, 847–881, 1985.
13. Zhao, A. P. and A. V. Räisänen, "Application of a simple and efficient source excitation technique to the FDTD analysis of waveguide and microstrip circuits," *IEEE Trans. Microwave Theory Tech.*, Vol. 44, No. 9, 1535–1539, 1996.
14. Pozar, D. M., *Microwave Engineering*, 2nd edition, Wiley, New York, NY, 1998.
15. Silver, S., *Microwave Antenna Theory and Design*, McGraw-Hill, New York, NY, 1949.
16. Van den Berghe, S., F. Olyslager, and D. De Zutter, "Efficient FDTD S-parameter calculation of microwave structures with TEM ports," *IEEE Ant. and Progat. Soc. Int. Symp.*, Orlando, FL, Vol. 2, 1078–1081, 1999.
17. Elliot, R. S., *Antenna Theory and Design*, Revised edition, Wiley, New York, NY, 2003.
18. Maloney, J. G., G. S. Smith, and W. R. Scott, "Accurate

computation of the radiation from simple antennas using the finite-difference time-domain method," *IEEE Trans. Ant. Propagat.*, Vol. 38, No. 7, 1059–1068, 1990.

19. Schneider, J. B., C. L. Wagner, and O. M. Ramahi, "Implementation of transparent sources in FDFD simulations," *IEEE Trans. Ant. Propagat.*, Vol. 46, No. 8, 1159–1168, 1998.

Jeffrey L. Young received the BSEE degree from Ohio Northern University in 1981, and the MSEE and Ph.D. degrees from the University of Arizona in 1984 and 1989, respectively. He was formerly a doctoral fellow and Staff Engineer with the Hughes Aircraft Company (1982–1991), Tucson, Arizona. He is currently a Professor Electrical and computer Engineering at the University of Idaho (1991–present) and lectures on electromagnetics, antenna theory and design, and microwave circuits. His research interests include electro-optical modulation, ferrite microwave devices, electromagnetic wave propagation in complex media and modern numerical methods in electromagnetics. He served nine years as an editor of the *IEEE Antennas and Propagation Magazine* and is currently serving as an elected member of the IEEE Antenna and Propagation Society Administrative Committee (2002–2004) and as the Antennas and Propagation Society Chapters Coordinator. In addition to these duties, he has served on numerous Technical Program Committees for the IEEE Antennas and Propagation International Symposium and has chair several technical sessions at the same. Professor Young is a a member of URSI (Commission B), a senior member of IEEE and a registered Professional Engineer in the State of Idaho.

Ryan Adams received the BSEE and BS Applied Mathematics degrees (*cum laude*) from the University of Idaho in 1999. He was formerly a developmental engineer with the United States Air Force. He is currently serving the Department of Electrical and Computer Engineering at the University of Idaho as a graduate research assistant. His research interests include electromagnetic wave propagation in complex media and high frequency circuits. He is a member of IEEE.